Materials Research. 2025; 28(suppl. 1): e20250138
DOI: https://doi.org/10.1590/1980-5373-MR-2025-0138

Characterization of a Gelcast AISI 310 SS Matrix Composite Reinforced by Alumina and GNP Particles

Louise Fernanda Rodrigues Oliveira*[a] , ***Fernando dos Santos Ortega*[b]** , ***Rodrigo Magnabosco*[c]** , ***Maurício David Martins das Neves*[a]**.

[a]*Comissão Nacional de Energia Nuclear (CNEN), Instituto de Pesquisas Energéticas e Nucleares (IPEN), São Paulo, SP, Brasil.*
[b]*Universidade do Vale do Paraíba (UNIVAP), Instituto de Pesquisa e Desenvolvimento (IP&D), São José dos Campos, SP, Brasil.*
[c]*Centro Universitário da FEI (FEI), Departamento de Engenharia de Materiais, São Bernardo do Campo, SP, Brasil.*

Received: January 11, 2025; Accepted: July 27, 2025

Gelcasting is a versatile forming technique suitable for preparing composite materials with various powders, including metallic and ceramic particles, at any solids concentration. Despite its potential, the application of gelcasting to produce metal matrix composites reinforced with alumina and graphene remains limited. This study investigates the gelcasting of AISI 310 stainless steel composites reinforced with 1, 3, and 5 vol.% nanosized alumina and 0.5 vol.% graphene nanoplatelets (GNPs). Rheological behavior and particle interactions were analyzed to ensure uniform dispersion. Thermal analysis determined optimal sintering conditions, avoiding densification issues. Compression and microhardness tests revealed yield strengths of up to 285 MPa at room temperature (RT) and 140 MPa at 800 °C, exceeding ASTM A351/A351M-18e1 standards. Microstructural refinement and homogeneous alumina distribution were achieved, with 3 vol.% alumina providing the best performance. The gelcasting process proved effective for producing dense, mechanically robust composites at a low cost.

Keywords: *Metal matrix composites, Gelcasting process, Powder metallurgy, AISI 310 stainless steel, Alumina, Graphene nanoplatelets.*

1. Introduction

The high demand for better, innovative and effective materials, manufactured by the best cost/benefit ratio as possible, is getting the materials science and engineering area to become closer to industry over the years[1]. In this context, composite materials of variable and multiple compositions are being developed in order to combine properties and meet the needs of the manufacturing project and materials specification[2].

Composites materials are made of a discontinuous phase (reinforcement) dispersed into a continuous phase (matrix), in variable volume ratio, shapes and distribution. Thus, mechanical, physical and chemical properties modifications may occur on matrix, adjusting it to determined engineering applications[1,3-5]. Composites are classified according to their matrix's nature, which could consist of ceramic, polymer or metal materials.

The gelcasting technique, initially designed for ceramic powders, consists of gelation, from a slurry of distilled water, organic binders and chemical reagents, in addition to the powders that are desired to work with[6,7]. After mixing, the slurry is verted into a mold, and after a few minutes of chemical reaction, the gelation occurs without any influence or assistance from external forces (i.e., compaction or injection), and the slurry takes the form of the mold[6]. Gelcasting itself demonstrated to be a low-cost technique, ease to apply to any kind of materials, including metal powders, while providing good superficial quality and also good process reproducibility[8], as demonstrated by Figure 1, in witch is possible to visualize the mold grooves printed on the green part (Figures 1a and 1b) and the smooth surface on the sintered part (Figure 1c).

Few studies have shown the application of this process to stainless steel powder materials have relevant and potential results, following what was achieved on the earlier stages with ceramic powders in terms of processing, and overcoming the same melted stainless steel values of yield strength resistance[9,10]. Nevertheless, some other authors have studied the production of metal matrix composites, with additions of ceramic particles as reinforcements in variable volumes percentages, using other fluid and powder processing techniques, showing promising and consistent results[3-5,11-16].

Both gelcasting and metal matrix composites (MMC) have been studied during the last decades. However, the application of gelcasting process to obtain MMC using ceramic particles as reinforcement is still scarce, particularly when the matrix is of stainless steel[8]. Colloidal processing techniques, such as gelcasting, could lead to well dispersion of reinforcements

*e-mail: louisefernandarodrigues@gmail.com
Associate Editor: Hamilton Abreu.
Editor-in-Chief: Luiz Antonio Pessan.

Figure 1. a) Stainless steel green part molded by gelcasting, 50 mL plastic cup as mold, side view; b) Stainless steel green part molded by gelcasting, 50 mL plastic cup as mold, bottom view; c) Stainless steel sintered part molded by gelcasting, (ø 14 mm x L 90 mm) cylindrical mold, side view.

Table 1. Chemical composition of AISI 310 stainless steel on weight percentage, according to technical data sheet supplied by ATMIX, with Fe bal.

Elem.	Ni	Cr	C	Si	Mn	Cu	Nb	P	S	Mo	Co	V	Sn
%	20.47	25.22	0.48	0.98	0.83	0.06	1.35	0.02	0.01	0.04	0.07	0.05	0.01

Table 2. Chemical composition of Al_2O_3 CT 3000 SG on weight percentage, according to technical data sheet supplied by ALMATIS.

Elem.	Al_2O_3	Na_2O	Fe_2O_3	SiO_2	MgO	CaO
%	99.800	0.030	0.015	0.015	0.040	0.015

along the matrix, moreover, to improve mechanical properties of the final part, with an extremely low manufacturing cost in comparison to other conventional techniques.

Notwithstanding the above mentioned about the easily application method, this could possibly be attributed to the differences between metallic and ceramic particles densities and shapes, what could lead to fast settling effect, if the rheology of the suspension is not controlled[10].

This work studies the use of the technique mentioned above to produce AISI 310 stainless steel matrix composites reinforced with additions of 1, 3 and 5 vol.% of alumina particles, in addition to 0.5 vol.% of graphene nanoplatelets (GNPs) particles, and its characterization in terms of microstructure and mechanical tests analysis.

2. Materials and Methods

2.1. Materials

The main components of all the compositions studied were AISI 310 stainless steel (HK-30, ATMIX), Al_2O_3 (CT-3000 SG, Almatis), and graphene Nanoparticles (GNP, Graphen Pesquisa e Tecnologia LTDA) powders. Their compositions are shown in Tables 1, 2, and 3.

Table 4 presents the other materials used to produce the composites developed and investigated in this study.

Table 3. Chemical composition of GNPs particles on weight percentage, according to data sheet supplied by Graphen P. T. LTDA.

Elem.	C	O	Other*
%	99.420	<0.050	0.576

*Other elements: K, Al, S, Ni, Cl, Si, Mg, Fe, Cr.

Table 4. Materials used to produce composites suspensions.

Material	Function
Metacrilamide (MAM)	Monomer
Polyethylene glycol – dimethacrylate (PEG-DMA)	Monomer
Sodium polyacrylate (Acumer 4800)	Dispersant
Polyvinylic alchool (PVAl)	Suspending agent
Ammonium persulfate (APS)	Initiator
N,N,N',N', thetrametylethylenediamine (TMED)	Catalist
Polyethylene glycol (PEG 800)	Drying
Lubricant oil	Demolding

2.2. Powder characterization

Laser diffraction technique (Microtrac BlueWave) was used to reveal the particle size measurements, as per ASTM E2651-

19 standard[17], and also, followed by density measurements using He picnometry (AccuPyc II 1340, Micromeritics).

Powders morphologies were viewed by SEM images (CamScan 3200 LV, Oxford Instruments; TM3000 Tabletop Microscope, HITACHI; and Mira3 LMH, TESCAM), both on loose condition.

2.3. Composites and specimen preparation, and density measurements

The composite suspensions and specimens followed the steps below for preparation, as shown in Figure 2. The compositions of each sample are in Table 5[8-10]. Even though some authors have used ball milling to mix powders and improve reinforcement particle dispersion on matrix[18-20], it was preferred to use a high-shear mixer to keep the stainless steel powder morphology. Once the suspensions were ready, they were poured into a cylindrical mold (90 mm high and 14 mm in diameter) for gelation.

After demolding, the gelcast parts were washed on tap water and then dried by osmosis in a 40 wt.% PEG solution for a couple of hours, to avoid undesirable cracks due to residual stress[21,22]. The drying step was finalized in an oven for 4 hours at 110 °C, and then the parts were sintered in an industrial furnace at 1280 °C for 1h in a vacuum atmosphere at 10^{-5} Torr to improve densification[10,23].

After sintering, cylinders were cut into specimens for compression tests (Figure 3), as per ASTM E9-09R18 and

Table 5. Composites compositions produced by gelcasting process.

Sample	Composition
I	AISI 310 puro
II	AISI 310 + 1 vol.% Al_2O_3
III	AISI 310 + 3 vol.% Al_2O_3
IV	AISI 310 + 5 vol.% Al_2O_3
V	AISI 310 + 0.5 vol.% GNP
VI	AISI 310 + 1 vol.% Al_2O_3 + 0.5 vol.% GNP
VII	AISI 310 + 3 vol.% Al_2O_3 + 0.5 vol.% GNP
VIII	AISI 310 + 5 vol.% Al_2O_3 + 0.5 vol.% GNP

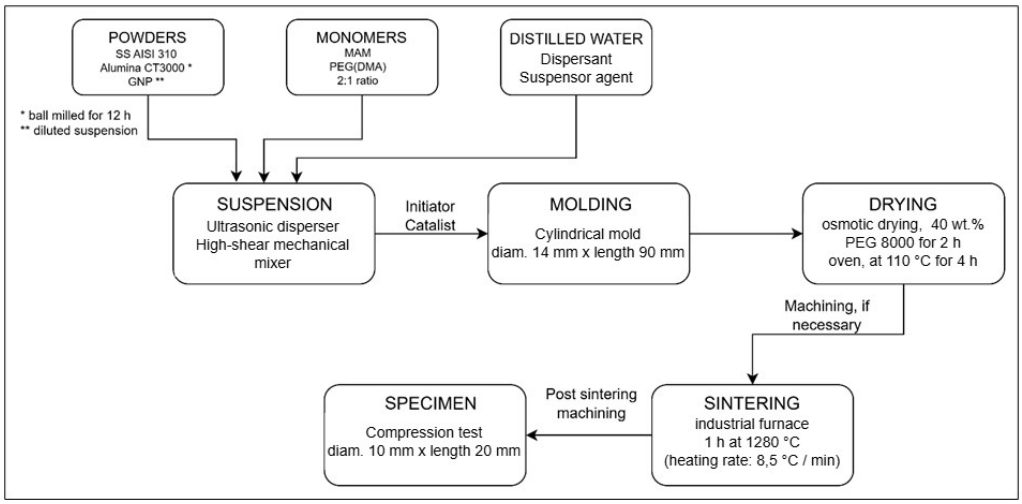

Figure 2. Suspensions and specimen preparation scheme.

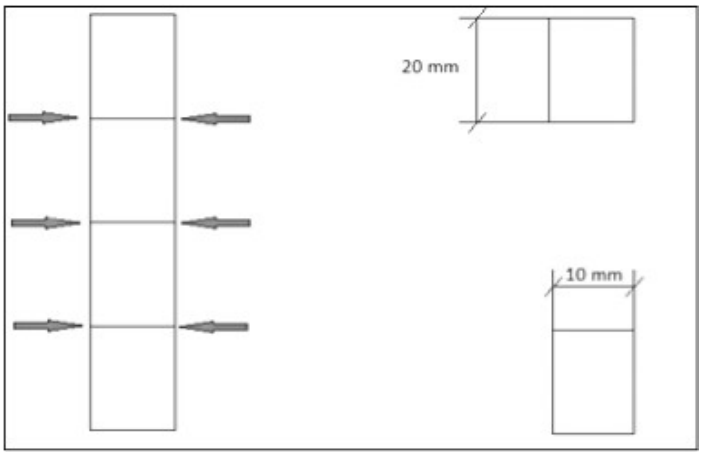

Figure 3. Specimen scheme preparation as per ASTM standard for compression tests at RT and 800 °C.

ASTM E209-18 standards[10,24,25]. Specimen densities were measured by He pycnometry and hydrostatic method, as per ASTM B962-17 standard[26].

2.4. Green compacts characterization

The weight loss of gelcast sample was measured by thermogravimetric analysis (TG-DSC Setsys Evolution 1750, SETARAM) before sintering. Debinding was expected to occur during the heating, without the need for a specific step for organic binders removal.

Sintering step was held in an industrial furnace, all the samples at the same time, to avoid external interferences, as stated in the previous section. The sintering temperature was under the liquidus phase limit of the stainless steel, which is 1300 °C.

2.5. Microstructure characterization

Microstructure characterization was led by optical microscopy (Axio Scope A1, Zeiss), field emission scanning electronic microscopy (JSM-6701F Field Emission Scanning Electron Microscope, Jeol), in addition to dispersion analysis and chemical elements mapping by energy dispersive spectroscopy (Noran System Six, Thermo Scientific). Also, x-ray diffraction (XRD 7000 X-Ray Diffractometer, Shimadzu) for quantitative analysis of the phases contained in the samples. All the samples were chemically etched with a 10 vol.% aqueous solution of oxalic acid (3 V, 1.5 mA for 3 s).

2.6. Compression and microhardness tests

Three specimens for each composition were randomly cut from any position of the sintered cylinder, as shown in Figure 3 scheme, and were tested at room temperature and 800 °C as per compression test standards[23,24]. A total of 48 tests (24 for each temperature) were considered to comply with statistical standard requests. The aim was to evaluate the settling effect after the gelcasting process and also to have the achieved results compared to values from ASTM A351/A351M-18e1 standard and other published work[27,28]. The tests were done in an MTS machine, with 5 mm of displacement, at 3 mm/min, considering a maximum load of 75 kN.

Microhardness test was carried out considering 10 random points of each sample, as per ASTM E384-17 standard[29], in an HMV-2 Shimadzu durometer.

3. Results and Discussion

3.1. Powder characterization

AISI 310 powder, was previously characterized by Oliveira et al[10]. It is a gas-atomized powder, and has spherical morphology with a few elongated particles, which could lead to favorable packaging during processing, and make the densification of the part to be easier and more effective. Al_2O_3 powder has irregular particles (Figure 4a), which could directly impact on packing and densification of parts after sintering. GNPs also have an irregular shape (Figures 4b and 4c), with little agglomerates of graphene platelets.

Powders densities, measured by pycnometry, are 7.571 g/cm^3, 3.980 g/cm^3 and 2.285 g/cm^3 for AISI 310, Al_2O_3 and GNPs respectively, following manufacturers' data (Table 6). The particle size distribution for both powders is shown on Table 6. AISI 310 with D_{50} = 10 µm, Al_2O_3 with D_{50} = 0.6 µm, and GNPs with layers of D_{50} = 10 µm (each layer with between 30-50 platelets of graphene). Reinforcement particles with irregular particles could directly affect the packaging and, therefore, impact microstructure refinement and mechanical properties of the material.

3.2. Green compacts characterization

The DSC/TGA and dilatometry analysis were both held in vacuum atmosphere until 1200 °C. These thermal tests indicated that at 400 °C the volatilization of organic binders is complete, and after 1100 °C the curve tendency

Table 6. Particle size distribution and density of both powders.

Material	Particle size D50 [µm]	Density [g/cm^3]
AISI 310	10	7.5709
Al_2O_3	0.6	3.9800
GNP	10 per layer / 30-50 platelets per layer	2.2850

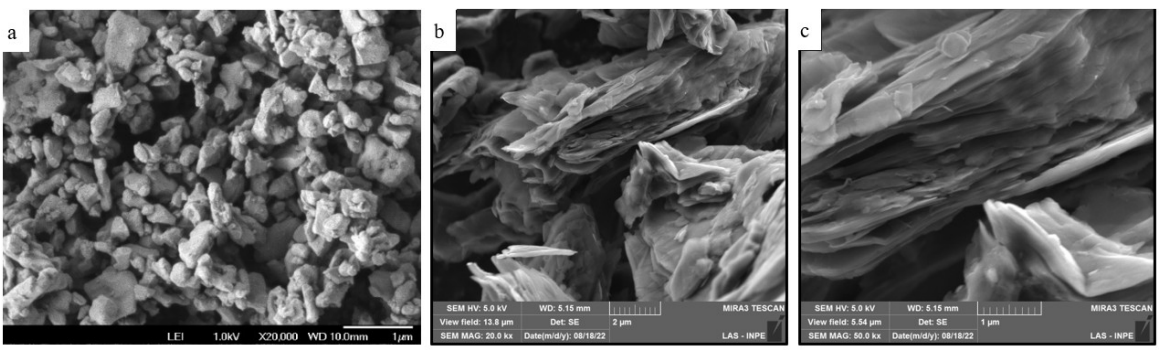

Figure 4. SEM images of a) Al_2O_3 powder in loose condition, with irregular shapes; b) GNPs particles as received, in a diluted suspension; c) GNPs particles on higher magnificent than b.

suggested that the heat flow was near to a constant value (Figures 5 and 6), following what was stated previously by Oliveira[8]. The temperature rate, also used in the sintering cycle, was adequate for this material, and it was then confirmed by ThermoCalc® simulation for the stainless steel (Figure 7).

Despite the particularities of each sample, as a function of the amount of reinforcements added to them, the profile of the curves has presented similar behavior of discreet retraction near 200 °C, followed by expansion and sharp retraction by 950 °C. The retraction rate found was about 15%, considering all the samples and compositions, which was considered satisfactory when compared to Oliveira[8]. The heat flow found on both samples, despite the reinforcements and their particle size, also followed similar behavior when compared to pure stainless steel. Variations by 500 °C and 1300 °C, related to some carbides formation were present in all samples analyzed, as predicted by the ThermoCalc® simulation, and which would be hereafter viewed on SEM images.

3.3. Specimen densities

The sintering retraction was calculated by measuring the samples before and after sintering, and the percentual differences on length and diameter dimensions are shown on Table 7. The retraction was predictable and isotropic for all samples, about 15%, following tendency found on literature[9,10].

All the samples achieved at least 94.50% of theoretical density (Table 8), which could be considered such an expressive result, since the materials processed were fine powders. For the pure stainless steel samples, results reached 99.50% of theoretical density, while the ones with the addition of GNPs reached 99.12%. It was observed that the sintered density increased slightly with the amount of reinforcements. Although similar data has been published for other kinds of stainless steel reinforced with alumina[30,31] or GNP[19,32], what could be a guide for comparison, the processing techniques were different. Additionally, no data for stainless steel using alumina and GNP reinforcements could be found.

The density results of each sample showed no apparent settling effect on processing, since there was no statistical difference between the specimens of the same composition, and the density of both samples was essentially the same along the vertical axis for each composition.

3.4. Microstructural characterization

SEM images of pure AISI 310 stainless steel (Figure 8a) showed to be similar to what was found in the literature for parts obtained by cast ingots of the same material[28,33]. Sintered samples reached 99% of theoretical density and images of

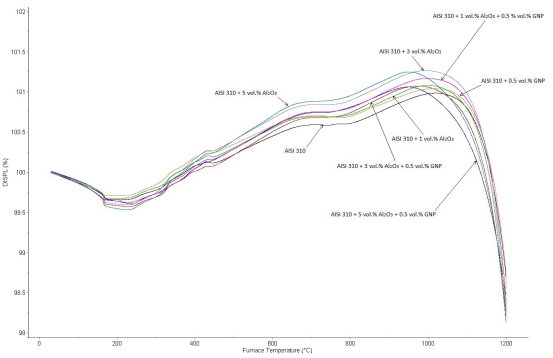

Figure 5. All samples dilatometry curves.

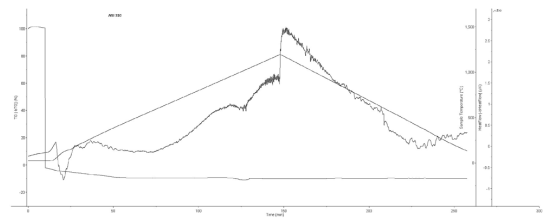

Figure 6. AISI 310 stainless steel DSC/TG curve.

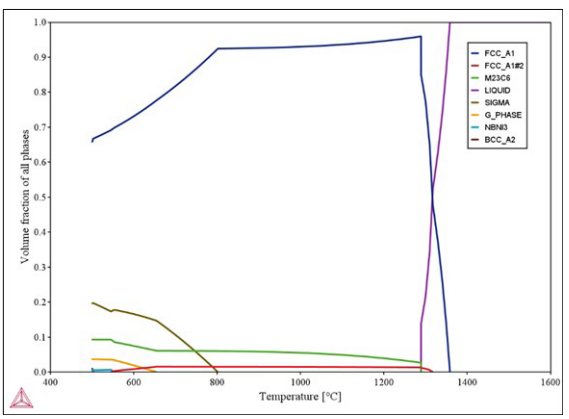

Figure 7. ThermoCalc® simulation of AISI 310 stainless steel.

Table 7. Percentual difference of dimensions and mass between pre and post sintering condition.

Samples	Lenght (%)	Diameter (%)	Mass (%)
I	-15.441	-15.966	-3.774
II	-15.593	-16.603	-3.677
III	-15.128	-15.811	-3.586
IV	-14.355	-15.393	-3.340
V	-16.169	-16.280	-3.702
VI	-15.064	-16.654	-3.925
VII	-15.801	-15.671	-3.573
VII	-15.966	-15.131	-3.456

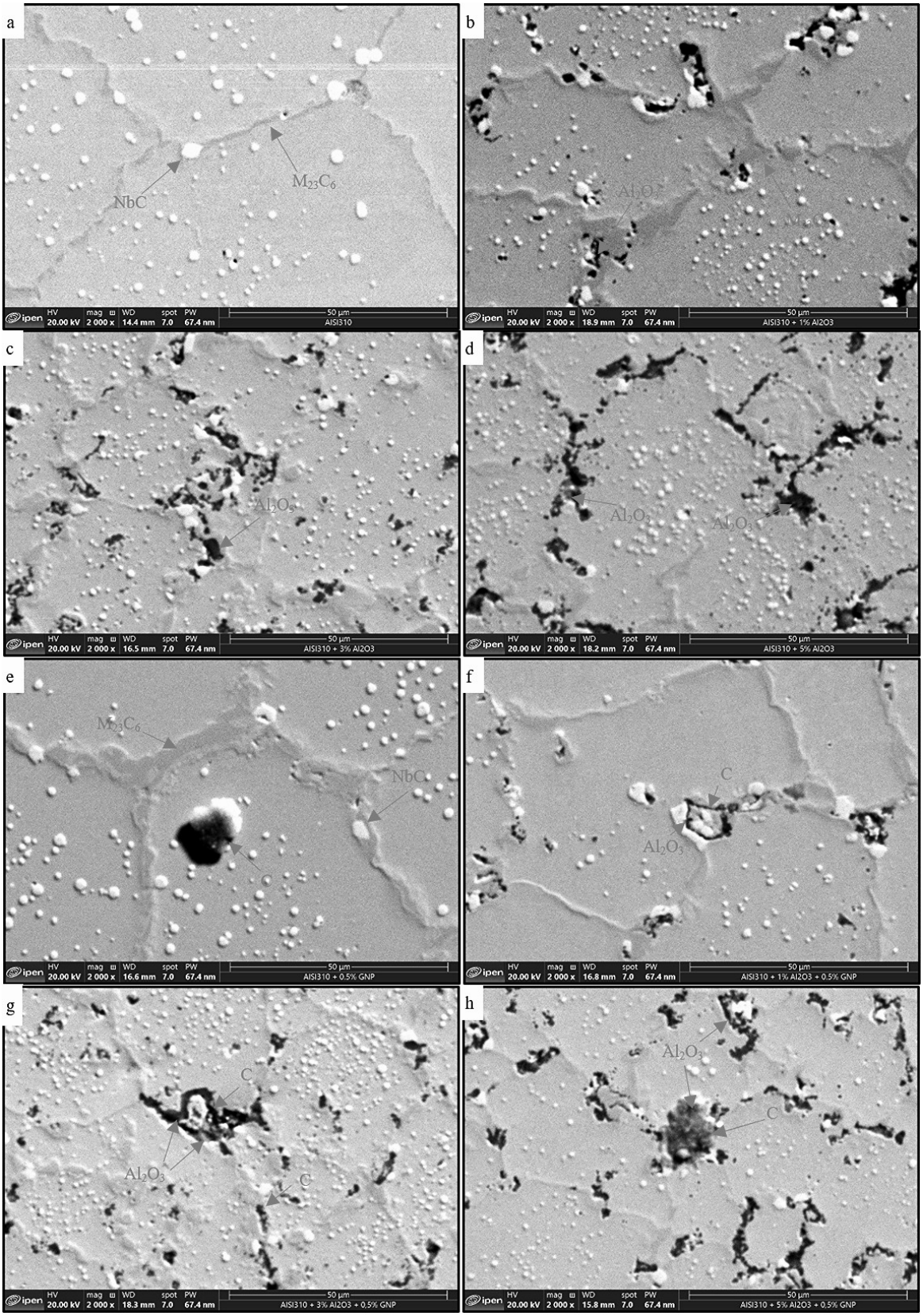

Figure 8. SEM images of the gelcast parts, with some carbides and reinforcements indications, a) AISI 310; b) AISI 310 + 1 vol.% Al_2O_3; c) AISI 310 + 3 vol.% Al_2O_3; d) AISI 310 + 5 vol.% Al_2O_3; e) AISI 310 + 0.5 vol.% GNPs; f) AISI 310 + 1 vol.% Al_2O_3 + 0.5 vol.% GNPs; g) AISI 310 + 3 vol.% Al_2O_3 + 0.5 vol.% GNPs; h) AISI 310 + 5 vol.% Al_2O_3 + 0.5 vol.% GNPs.

the polished surface did not reveal the presence of pores in the microstructure. The samples that included alumina and graphene nanoplatelet (GNP) particles exhibited a refinement in microstructure as the amount of reinforcement increased. This phenomenon occurs due to the restrictions imposed against the movement of grain boundaries within the stainless steel matrix (see Figures 8b-h). These restrictions prevent grain coalescence during the sintering process. This observation aligns with findings from other authors who have reported similar effects when using alumina and graphene as mechanisms for hardening and microstructure refinement in AISI 316L stainless steel, nickel, and aluminum matrix composites[18-20].

The EDS and mapping elements results showed that there are some NbC carbides (white dots) throughout the entire length of the matrix, and $M_{23}C_6$ carbides (CrC carbides) on the grain boundaries regions. On samples containing reinforcements additions, alumina particles were found to be near the necks and some pores, justifying and endorsing the smaller results of these samples density. Despite some pores were found on the samples, the reinforcement particles have a satisfactory dispersion through the stainless steel matrix.

X-ray diffraction patterns presented a strong presence of austenitic phase, with some peaks of NbC and CrC carbides. In samples with alumina additions, discreet aluminum peaks were observed. The additions of graphene were too small to identify this phase in the samples with this reinforcement (Figure 9).

3.5. Mechanical properties

Specimens were randomly tested, regardless of their position on the cylindrical mold. One of the implicit objectives of this work was to evaluate various issues, including the settling effect of the powders during processing and its potential impact on mechanical properties and microstructures. To achieve this, a compression test was selected. Additionally, tension tests at 800 °C would require larger specimens, as the entire tested assembly would need to be fully immersed in the high-temperature environment, a limitation imposed by the equipment used. Furthermore, aside from the direction of load application, compression and tension tests can be compared up to the yield strength limit, as the elastic behavior in both tests yields similar results for the modulus of elasticity and yield strength[34].

The results of the room temperature and 800 °C compression tests are presented in Figure 10. These results were then compared to the values established by ASTM A351/A351M-14[27] for room temperature (RT) and to the work of Ekström and Jonsson[28] for the 800 °C tests.

At room temperature, all samples with only alumina additions achieved the target yield strength of 240 MPa. The pure AISI 310 stainless steel reached 98.62% of this target. However, among the samples with graphene nanoplatelet (GNP) additions, only those with 3 and 5 vol.% of alumina met the expected standard. Notably, these samples still performed worse than their counterparts without GNPs. These results can be attributed to several factors, including the densification of the materials, the restrictions caused by the rigid reinforcement particles, and the size discrepancies between the matrix particles and the reinforcements. This led to a higher incidence of voids among the stainless steel, alumina, and graphene particles.

Specimens containing 1 and 3 vol.% of alumina particles, both achieving over 98% of the theoretical density of the composite, exhibited yield strengths of 258.34 MPa and 261.67 MPa, respectively. These results are quite similar to those obtained by Li et al[35], who processed AISI 316L stainless steel using selective laser melting and employed the same alumina particles for reinforcement.

Although some other authors have successfully enhanced the yield strength of nickel and aluminum matrices by adding graphene nanoplatelets (GNPs) particles[19,36,37], this effect was not observed in this research, at least for room temperature (RT) tests. The methods used in those studies were selective laser melting and high-energy ball milling for powder mixing. These techniques may have improved the interaction between the composite particles, directly impacting the enhancement of mechanical properties in those other studies.

In the case of compression tests at 800 °C, the specimens that included alumina and graphene nanoplatelets (GNPs) performed better than those without any reinforcements. While the samples made from pure AISI 310 stainless steel (SS) and those containing only GNPs were found to be over 99% of theoretical density, the superior performance of the composites with additional reinforcements is attributed to the thermal stability of these materials and the improved interaction between the reinforcements and the stainless steel particles at elevated temperatures. AISI 310 SS is recognized for its favorable properties in high-temperature environments, where strong oxidation, corrosion, and fatigue resistance are essential.

The formation of precipitates due to high temperatures can lead to material hardening, which is enhanced by the high nickel and chromium content in its composition. These properties, as well as methods to enhance them, have been the subject of research by various authors for several years[33,38-42]. However, the use of a combination of reinforcements, as demonstrated in this study, remains relatively rare in the literature.

The results of the Vickers microhardness test are presented in Table 9. Although the values obtained were lower than the reported value of 276 HV1 from Gunes and Yildiz[40], they were more in line with the findings of Ortega et al[43], who produced gelcast parts using the same AISI 310 stainless steel, achieving values around 210 to 233 HV1. The discrepancy between the values in the literature and those found in this study may be attributed to the porosity observed in the microstructure and density analysis.

Among the samples that contained only alumina additions, the one with 3 vol.% alumina achieved the highest hardness value of 192.8 HV1. In contrast, the samples with 1 vol.% and 5 vol.% alumina, as well as those with 0.5 vol.% GNPs and 5 vol.% alumina, exhibited the lowest hardness results. Notably, the samples with only GNPs addition attained the greatest hardness value, indicating a strong interaction between the stainless steel and graphene particles, as demonstrated in the micrographs.

Although no study has been conducted on the tribological properties of these composites or their wear resistance, the results suggest that further research varying the volume fraction of graphene added could be a promising way to investigate these properties.

Table 8. Density results from samples pre and post sintering step,

Samples	Theoretical	Pre-sinter. (geometr.)	Post-sinter. (hidrost.)	% theoretical and sintered
I	7.800	4.679	7.761	99.50%
II	7.760	4.628	7.656	98.66%
III	7.680	4.612	7.550	98.31%
IV	7.600	4.575	7.277	95.75%
V	7.772	4.436	7.704	99.12%
VI	7.732	4.428	7.564	97.82%
VII	7.652	4.422	7.491	97.89%
VII	7.572	4.430	7.170	94.69%

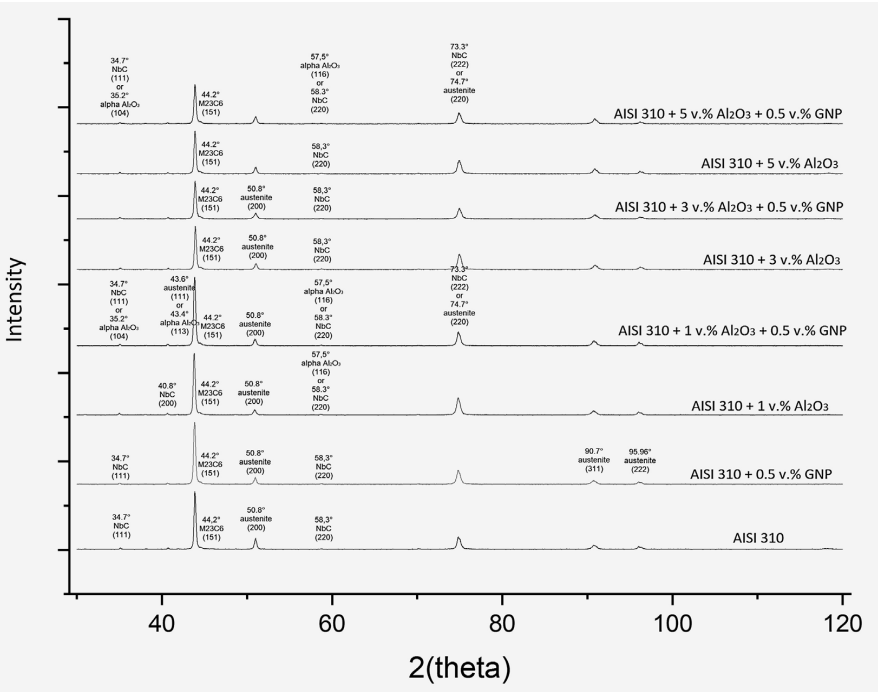

Figure 9. XRD patterns of gelcast samples.

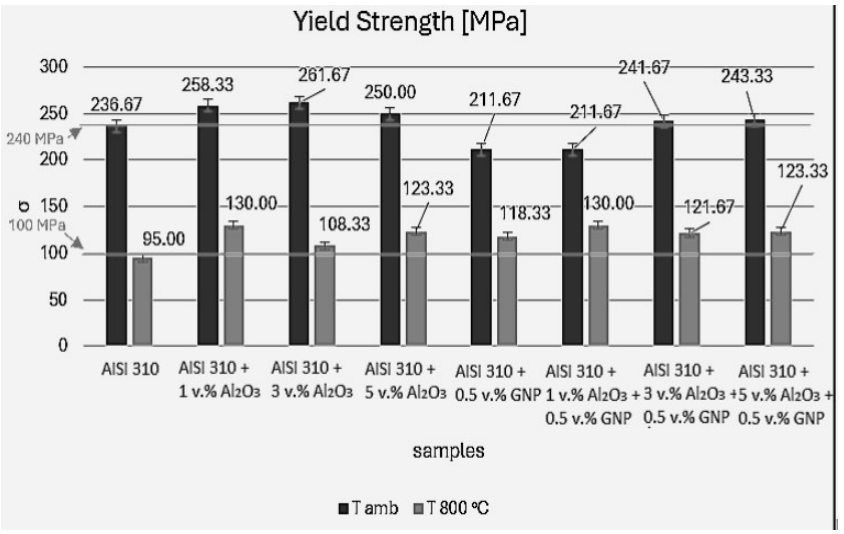

Figure 10. Yield strength results for RT (T amb, blue bars) and 800 °C (T 800 °C, orange bars) compression tests, with the target values of 240 MPa and 100 MPa, respectively, indicated.

Table 9. Vickers microhardness test results of gelcast composites samples.

Samples	Vickers Microhardness [HV_1]
I	187,4
II	184,9
III	192,8
IV	182,9
V	200,6
VI	188,0
VII	188,3
VII	177,5

Testing samples for the mechanical tests were cut from various positions of the molded cylinders, and no significant differences were identified in the values of density, yield stress, and hardness that could be attributed to the effect of sedimentation.

4. Conclusions

This study demonstrated the successful application of gelcasting to produce AISI 310 stainless steel matrix composites reinforced with alumina and graphene nanoplatelet (GNP) particles. Key findings include:

- The addition of reinforcements improved microstructural refinement, with alumina and GNPs restricting grain growth and enhancing dispersion within the matrix.
- Samples achieved high densification (above 94.5% of theoretical density), with minimal porosity affecting mechanical performance. Pure AISI 310 and GNP-only samples reached densities above 99%.
- At room temperature, composites with 1% and 3% alumina additions achieved superior yield strengths, outperforming pure AISI 310. At 800 °C, composites with alumina and GNPs exhibited enhanced thermal stability and mechanical strength, outperforming non-reinforced samples.
- The addition of reinforcements slightly reduced hardness compared to pure stainless steel but remained within acceptable ranges for practical applications.

These results validate the gelcasting process as a viable, low-cost technique for producing advanced stainless steel composites with tailored properties, suitable for high-temperature applications.

5. Acknowledgments

The authors thank IPEN, FEI, UNIVAP and BRATS for their institutional support and complete structure for carrying out this research, in addition to CNPq for partial financial support.

6. References

1. Samal PK, Newkirk JW, editors. ASM Handbook: powder metallurgy. Cleveland: ASM International; 2015. 907 p. (vol. 7). http://doi.org/10.31399/asm.hb.v07.9781627081757
2. Levy F No, Pardini LC. Compósitos estruturais: ciência e tecnologia. 2. ed. São Paulo: Edgar Blücher; 2016. 416 p.
3. Feizabadi J, Khaki JV, Sabzevar MH, Sharifitabar M, Sani SA. Fabrication of in situ Al_2O_3 reinforced nanostructure 304 stainless steel matrix composite by self-propagating high temperature synthesis process. Mater Des. 2015;84:325-30. http://doi.org/10.1016/j.matdes.2015.06.138.
4. Cui C, Schulz A, Uhlenwinkel V, Zoch HW. Spray-formed stainless steel matrix composites with co-injected carbide particles. Metall Mater Trans, A Phys Metall Mater Sci. 2011;42(8):2442-55. http://doi.org/10.1007/s11661-011-0633-z.
5. Kan WH, Ye ZJ, Zhu Y, Bhatia VK, Dolman K, Lucey T, et al. Fabrication and characterization of microstructure of stainless steel matrix composites containing up to 25vol.%NbC. Mater Charact. 2016;119:65-74. http://doi.org/10.1016/j.matchar.2016.07.019.
6. Janney MA. Gelcasting superalloy powders: metals and ceramic division. Oak Ridge: Oak Ridge National Laboratory; 1996.
7. Janney MA, Omatete OO, Walls CA, Nunn SD, Ogle RJ, Westmoreland G. Development of low-toxicity gelcasting systems. J Am Ceram Soc. 1998;81(3):581-91. http://doi.org/10.1111/j.1151-2916.1998.tb02377.x.
8. Oliveira LFR. Caracterização de compósitos de matriz de aço inoxidável AISI 310 reforçado com partículas de alumina e grafeno processado por gelcasting [thesis]. São Paulo: Instituto de Pesquisas Energéticas e Nucleares, IPEN-CNEN, Universidade de São Paulo; 2024, 167 p.
9. Oliveira LFR. Avaliação microestrutural e do comportamento termomecânico do aço inoxidável HK-30 conformado por gelcasting [dissertation]. São Bernardo do Campo: Centro Universitário da FEI; 2015, 86 p.
10. Oliveira LFR, Neves MDM, Ortega FS. AISI 310 stainless steel formed by gelcasting: an alternative manufacture method. Mater Sci Forum. 2020;1012:325-30. http://doi.org/10.4028/www.scientific.net/MSF.1012.325.
11. Basak AK, Pramanik A, Islam MN, Anandakrishnan V. Challenges and recent developments on nanoparticle-reinforced metal matrix composites. In: Dong Y, Umer R, Lau AKT, editors. Fillers and reinforcements for advanced nanocomposites. Sawston: Woodhead Publishing; 2015. p. 349-367. http://doi.org/10.1016/B978-0-08-100079-3.00014-4
12. Candelario VM, Guiberteau F, Moreno R, Ortiz AL. Aqueous colloidal processing of submicrometric SiC plus Y3Al5O12 with diamond nanoparticles. J Eur Ceram Soc. 2013;33(13-14):2473-82. http://doi.org/10.1016/j.jeurceramsoc.2013.04.016.
13. Escribano JA, García JL, Alvaredo P, Ferrari B, Gordo E, Sánchez-Herencia AJ. FGM stainless steel-Ti(C,N) cermets through colloidal processing. Int J Refract Hard Met. 2015;49:143-52. http://doi.org/10.1016/j.ijrmhm.2014.05.008.
14. He F. Ceramic nanoparticles in metal matrix composites. In: Banerjee R, Manna I, editors. Ceramic nanocomposites. Sawston: Woodhead Publishing; 2013. p. 185-207. http://doi.org/10.1533/9780857093493.2.185
15. Huang L, Liu R, Wang Y, Zhang C, Long X, Cao Y. Fabrication and properties of dense silicon carbide ceramic via gel-casting and gas silicone infiltration. Ceram Int. 2016;42(16):18547-53. http://doi.org/10.1016/j.ceramint.2016.08.194.
16. Ibrahim MF, Ammar HR, Samuel AM, Soliman MS, Samuel FH. On the impact toughness of Al-15vol.%B4C metal matrix composites. Compos, Part B Eng. 2015;79:83-94. http://doi.org/10.1016/j.compositesb.2015.04.018.
17. ASTM: American Society for Testing and Materials. ASTM E2651-19: standard guide for powder particle size analysis. West Conshohocken: ASTM International; 2019.
18. Das A, Yadav V, Almangour B, Prasad HC, Sathish N, Ashiq M, et al. Additive manufacturing of graphene reinforced 316L stainless steel composites with tailored microstructure and mechanical properties. Mater Chem Phys. 2023;303:127826. http://doi.org/10.1016/j.matchemphys.2023.127826.
19. Patil A, Nartu MSKKY, Ozdemir F, Banerjee R, Gupta RK, Borkar T. Enhancement of the mechanical properties

of graphene nanoplatelet (GNP) reinforced nickel matrix nanocomposites. Mater Sci Eng A. 2021;817:141324. http://doi.org/10.1016/j.msea.2021.141324.
20. Tabandeh-Khorshid M, Ferguson JB, Schultz BF, Kim CS, Cho K, Rohatgi PK. Strengthening mechanisms of graphene- and Al2O3-reinforced aluminum nanocomposites synthesized by room temperature milling. Mater Des. 2016;92:79-87. http://doi.org/10.1016/j.matdes.2015.12.007.
21. Barati A, Kokabi M, Famili MHN. Drying of gelcast ceramic parts via the liquid desiccant method. J Eur Ceram Soc. 2003;23(13):2265-72. http://doi.org/10.1016/S0955-2219(03)00045-1.
22. Trunec M. Osmotic drying of gelcast bodies in liquid desiccant. J Eur Ceram Soc. 2011;31(14):2519-24. http://doi.org/10.1016/j.jeurceramsoc.2011.02.015.
23. Ji CH, Loh NH, Khor KA, Tor SB. Sintering study of 316L stainless steel metal injection molding parts using Taguchi method: final density. Mater Sci Eng A. 2001;311(1-2):74-82. http://doi.org/10.1016/S0921-5093(01)00942-X.
24. ASTM: American Society for Testing and Materials. ASTM E9-09R18: standard test methods of compression testing of metallic materials at room temperature. West Conshohocken: ASTM International; 2018.
25. ASTM: American Society for Testing and Materials. ASTM E209-18: standard practice for compression tests of metallic materials at elevated temperatures with conventional or rapid heating rates and strain rates. West Conshohocken: ASTM International; 2018.
26. ASTM: American Society for Testing and Materials. ASTM B962-17: standard test methods for density of compacted or sintered powder metallurgy (pm) products using Archimedes' principle. West Conshohocken: ASTM International; 2017.
27. ASTM: American Society for Testing and Materials. ASTM A351/A351M-18e1: standard specification for castings, austenitic, for pressure-containing parts. West Conshohocken: ASTM International; 2019.
28. Ekström M, Jonsson S. High-temperature mechanical – and fatigue properties of cast alloys intended for use in exhaust manifolds. Mater Sci Eng A. 2014;616:78-87. http://doi.org/10.1016/j.msea.2014.08.014.
29. ASTM: American Society for Testing and Materials. ASTM E384-17: standard test method for knoop and vickers hardness of materials. West Conshohocken: ASTM International; 2021.
30. Nie D, Mutoh Y. Fatigue limit prediction of the matrix of 17-4PH stainless steel based on small crack mechanics. J Press Vessel Technol. 2013;135(2):021407. http://doi.org/10.1115/1.4023428.
31. Allabergenov B, Tursunkulov O, Abidov A, Jeong S, Kim S. Mechanical properties of stainless steel composites with titanium carbonitride consolidated by spark plasma sintering. J Compos Mater. 2016;50(12):1567-72. http://doi.org/10.1177/0021998315574756.
32. Patel RB, Liu J, Scicolone J, Roy S, Mitra S, Dave RN, et al. Formation of stainless steel-carbon nanotube composites using a scale chemical vapor infiltration process. J Mater Sci. 2013;48(3):1387-95. http://doi.org/10.1007/s10853-012-6885-1.
33. Xiang S, Jonsson S, Zhu B, Odqvist J. Corrosion fatigue of austenitic cast iron Ni-Resist D5S and austenitic cast steel HK30 in argon and synthetic diesel exhaust at 800 °C. Int J Fatigue. 2020;132:105396. http://doi.org/10.1016/j.ijfatigue.2019.105396.
34. Dowling NE, Kampe S, Kral M. Mechanical behavior of materials. 5. ed. New Jersey: Prentice Hall; 2019. 992 p.
35. Li X, Willy HJ, Chang S, Lu W, Herng TS, Ding J. Selective laser melting of stainless steel and alumina composite: experimental and simulation studies on processing parameters, microstructure and mechanical properties. Mater Des. 2018;145:1-10. http://doi.org/10.1016/j.matdes.2018.02.050.
36. Khanna V, Kumar V, Bansal SA. Effect of reinforcing graphene nanoplatelets (GNP) on the strength of aluminium (Al) metal matrix nanocomposites. Mater Today Proc. 2022;61(2):280-5. http://doi.org/10.1016/j.matpr.2021.09.227.
37. Rashad M, Pan F, Tang A, Asif M. Effect of graphene nanoplatelets addition on mechanical properties of pure aluminum using a semi-powder method. Prog Nat Sci. 2014;24(2):101-8. http://doi.org/10.1016/j.pnsc.2014.03.012.
38. Bahrami A, Ashrafi A, Rafiaei SM, Mehr MY. Sigma phase-induced failure of AISI 310 stainless steel radiant tubes. Eng Fail Anal. 2017;82:56-63. http://doi.org/10.1016/j.engfailanal.2017.08.027.
39. Garcia JM, Monteiro ACA, Casanova AMB, Huaman NRC, Monteiro SN, Brandão LP. Microstructural analysis of phase precipitation during high temperature creep in AISI 310 stainless steel. J Mater Res Technol. 2023;23:5953-66. http://doi.org/10.1016/j.jmrt.2023.02.175.
40. Gunes I, Yildiz I. Investigation of adhesion and tribological behavior of borided AISI 310 stainless steel. Materia. 2016;21(1):61-71. http://doi.org/10.1590/S1517-707620160001.0006.
41. Queiroga LR, Marcolino GF, Santos M, Rodrigues G, Santos CE, Brito P. Influence of machining parameters on surface roughness and susceptibility to hydrogen embrittlement of austenitic stainless steels. Int J Hydrogen Energy. 2019;44(54):29027-33. http://doi.org/10.1016/j.ijhydene.2019.09.139.
42. Sun H, Sun Y, Zhang R, Wang M, Tang R, Zhou Z. Study on hot workability and optimization of process parameters of a modified 310 austenitic stainless steel using processing maps. Mater Des. 2015;67:165-72. http://doi.org/10.1016/j.matdes.2014.11.041.
43. Ortega FS, Oliveira RLS, Plínio MC, Nobrega BN. Gelcasting of stainless steel powder: an alternative to injection molding. Mater Sci Forum. 2010;660-661:194-9. http://doi.org/10.4028/www.scientific.net/MSF.660-661.194.

Data Availability

The datasets generated during the current study are not publicly available but are available from the corresponding author on reasonable request.